Electronic Supplementary Information

MOF (UiO-66-NH_2)@COF (TFP-TABQ) Hybrids via On-surface Condensation Reactions for Sustainable Energy Storage

Dawid Pakulski,[a,b*] Veronica Montes-García,[c] Wlodzimierz Czepa,[d] Dawid Marcinkowski,[d] Haijun Peng,[c] Tomasz Chudziak,[d] Adam Gorczyński,[d] Wojciech Kukułka,[c] Cataldo Valentini,[a] Violetta Patroniak,[d] Paolo Samorì,[c*] Artur Ciesielski[a,c*]

[a.] Centre for Advanced Technologies, Adam Mickiewicz University, Uniwersytetu Poznańskiego 10, 61-614 Poznań, Poland Email: dawid.pakulski@amu.edu.pl
[b.] Adam Mickiewicz University Foundation, Poznań Science and Technology Park, Rubież 46, 61-612 Poznań, Poland
[c.] Université de Strasbourg, CNRS, ISIS 8 allée Gaspard Monge, 67000 Strasbourg, France Email: samori@unistra.fr, ciesielski@unistra.fr
[d.] Faculty of Chemistry, Adam Mickiewicz University, Uniwersytetu Poznańskiego 8, 61-614 Poznań, Poland

Table of Contents

Section A. Material Characterization:

The following materials were procured for the study: 2-Aminoterephthalic acid, zirconium chloride, polyvinylpyrrolidone, 1-Ethyl-3-methylimidazolium chloride, propylene carbonate, trifluoroacetic acid, acetic acid, separators in the form of Whatman® glass microfiber filters, binder poly(tetrafluoroethylene) (PTFE), and 1-methyl-2-pyrrolidinone (NMP) were all sourced from Sigma Aldrich. Conductive Carbon Black Super P (H30253) was obtained from Alfa Aesar, and the carbon AvCarb P75 substrate was supplied by FuelCellStore.

The **^{13}C nuclear magnetic resonance (NMR)** spectra of MOF, COF, and MOF@COF were recorded using a Bruker Avance III HD NMR spectrometer. **Powder X-ray diffraction (PXRD)** patterns were recorded with a Bruker ASX D8 Advanced X-ray diffractometer, utilizing Cu Kα line focused radiation (λ = 1.5405 Å). Surface areas and porosity were determined by conducting nitrogen adsorption and desorption at 77 K using a **Micromeritics ASAP 2050**. Prior to analysis, the samples were degassed under vacuum at 100 °C for 12 hours. Infrared spectra were acquired with a **Fourier infrared spectrometer (FT-IR)**-4700 JASCO, equipped with an ATR Diamond attachment, in the mid-IR range of 500−3700 cm^{-1}. **Thermogravimetric analysis (TGA)** for all samples was conducted on a Mettler Toledo TGA/SDTA851e system, covering a temperature range from 25 to 900 °C under an N_2 atmosphere, with a heating rate of 5 °C min^{-1}. **Scanning electron microscopy (SEM)** images were obtained using an FEI Quanta 250 FEG Scanning Electron Microscope, operating at an accelerating voltage of 30 keV for the incident beam energy. **X-ray photoelectron spectroscopy (XPS)** was performed using a Thermo Scientific KAlpha X-ray photoelectron spectrometer with a monochromatized Al Kα anode as the X-ray source (1.486 eV).

Synthesis of MOF-UIO-66-NH_2.

2-Aminoterephthalic acid (NH_2-BDC) (0.54 g, 3 mmol) and $ZrCl_4$ (0.5 g, 2 mmol) were dissolved in 40 mL of DMF and sonicated for 30 minutes. Then, 1 g of polyvinylpyrrolidone (PVP) was added to the mixture and subsequently sonicated for 30 minutes. The mixed solution, which became transparent, was transferred into a 100 mL round-bottom flask for the hydrothermal treatment at 120 °C for 24 hours. After being cooled to room temperature, the resultant suspension was centrifuged and rinsed with DMF, acetone, and ethanol three times, and then the product was activated with anhydrous acetone for 3 days and dried in a vacuum oven at 120 °C for 12 hours. Yield: 86%.

Synthesis of COF TPF-TABQ

The synthesis COF (TPF-TABQ) was conducted according to the following procedure. Typically, TFP (63 mg, 0.3 mmol) and TABQ (75,6 mg, 0.45 mmol) were dissolved in anhydrous 1,4-dioxane with acetic acid (3 M, 1 mL) in a glass vial (10 mL). The above mixture was sonicated for 10 minutes, then degassed through 3 freeze–pump–thaw cycles and the vial was flame sealed and heated at 120 °C for 3 days. The precipitate was collected *via* centrifugation, washed 3 times with anhydrous THF and methanol. The collected powder was dried at 120 °C under vacuum overnight to get brown TPF-TABQ. Yield: 93 %.

Synthesis of the MOF@COF hybrid.

The MOF@COF hybrid porous material was prepared by adding 60 mg of MOF-UIO-66-NH_2 powder and 16 mg (0,076 mmol) of 1,3,5-triformylphloroglucinol to 4 mL of 1,4- dioxane solution. The mixture was sonicated for 30 minutes and heated at 80 °C for 2 hours in an oil bath under vigorous stirring. Then, 0.5 mL of acetic acid (3 M) was added dropwise to the suspension under stirring, during which the mixture solution became brighter. 2 mL of a 1,4-dioxane solution containing 19,2 mg (0,114 mmol) of tetraminobenozquinone (TABQ) was added with a speed of 100 µl/min and continued stirring for 1 hour. The vial was then degassed through three freeze−pump−thaw cycles, and the vial was sealed and heated at 120 °C for 3 days. The resulting product was collected at room temperature by means of centrifugation and washed with acetone, tetrahydrofuran, and methanol and dried under vacuum. Yield: 87 %.

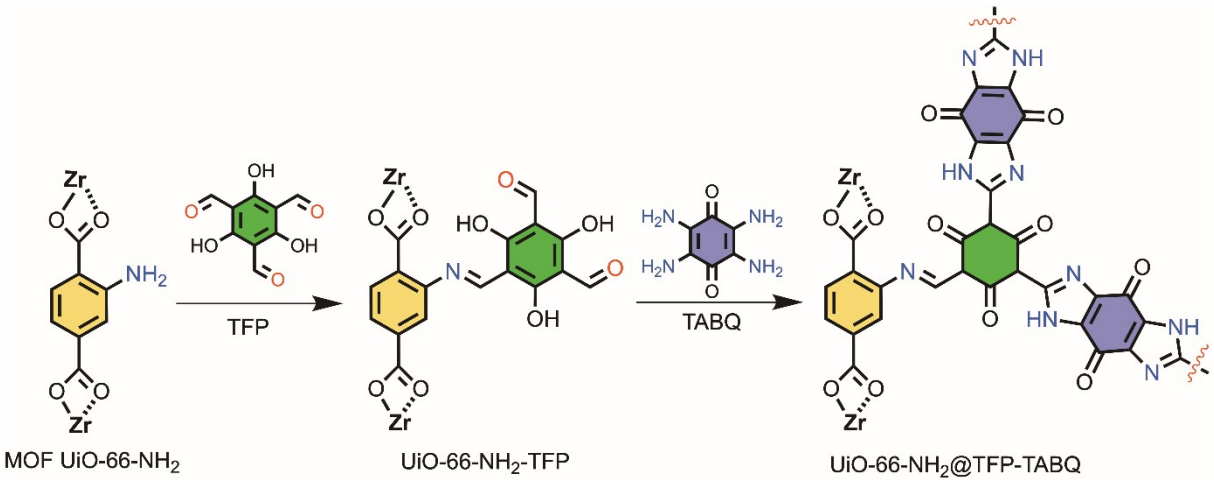

Fig. S1 The synthetic route of MOF@COF hybrids.

Electrochemical measurements:

The electrochemical performance of the MOF,COF, MOF@COF electrodes including cyclic voltammetry (CV), galvanostatic charge/discharge (GCD) profiles and electrochemical impedance spectroscopy (EIS) were evaluated in CR2032 type coin cells at room temperature using a EC-LAB VMP3 (BioLogic Science Instrument).

Electrodes preparation and electrochemical measurements

Fabrication of working electrodes: The working electrodes were prepared by mixing of active material (MOF,COF and MOF@COF) (80% wt, 16 mg), carbon black (10% wt, 2 mg) and PTFE (10% wt, 2 mg) in agate mortar with several drops of NMP to obtain a homogenous paste. The paste was then coated into a carbon paper electrode with diameter of 1.6 cm and further dried under vacuum at 80° C. The mass loading of the MOF,COF and MOF@COF was ~1 mg/cm^2 in each electrode.

Fabrication of symmetrical two-electrode configuration: Two electrodes were assembled in CR2032 stainless steel coin-type cells with a porous cellulose membrane as separator and 1M 1-Ethyl-3-methylimidazolium chloride in propylene carbonate as electrolyte.

Electrochemical characterization of the symmetric cell: CV was performed in the voltage range from 0 to 1.6 V for MOF and from 0 to 2 V for COF and MOF@COF using scan rates ranging from 2 to 500 mV/s. GCD was performed in the same voltage windows using current densities varying from 0.5 to 2 A/g. Cyclability tests were performed through GCD measurements at 1 A/g scan rate for 2000 cycles in the same potential windows.

Electrochemical calculations

Calculation of the specific capacitances: The specific capacitance was calculated using GCD with following equation:

$$C_s = \frac{2 \cdot I \cdot \Delta t}{\Delta V \cdot m} \qquad \text{(eq. 1)}$$

Where, I (A) is the response current, Δt (s) is the discharge time, ΔV (V) is the voltage window and m (g) is the mass of MOF,COF or MOF@COF in a single electrode.

Power and energy density calculations

The energy density of the device was obtained from the formula:

$$E = \frac{1}{2} \cdot C \cdot \frac{(\Delta V)^2}{3.6} \qquad \text{(eq. 2)}$$

The power density of the device was calculated from the formula:

$$P = \frac{E}{\Delta t} \cdot 3600 \qquad \text{(eq. 3)}$$

Where, E is specific energy (Wh kg^{-1}), C is the specific capacitance (F/g), ΔV is the potential window (V), P is power density (W kg^{-1}) and Δt is the discharge time (s).

Calculations for the kinetics the electrochemical processes occurring at both electrode materials:

$$i = av^b. \qquad \text{(eq. 4)}$$

Where i is the peak current and v the scan rate.

$$i = k_1v + k_2v^{1/2} \qquad \text{(eq. 5)}$$

Where k_1v and $k_2v^{1/2}$ represent the capacitive and diffusion limited effects, respectively.

Calculation of ionic conductivity (σ)

$$\sigma = \frac{l}{R_i \cdot A} \qquad \text{(eq. 6)}$$

Being l the film thickness (100 μm), A the film area (1.27 cm^2) and Rs is the ionic resistance.

Section B. Physical characterization

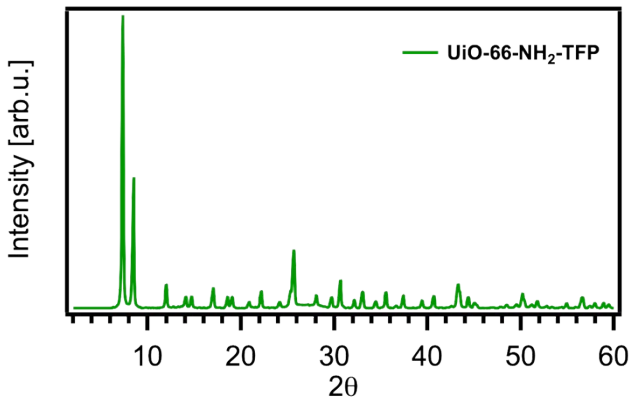

Figure S2. PXRD of UiO-66-NH_2-TFP.

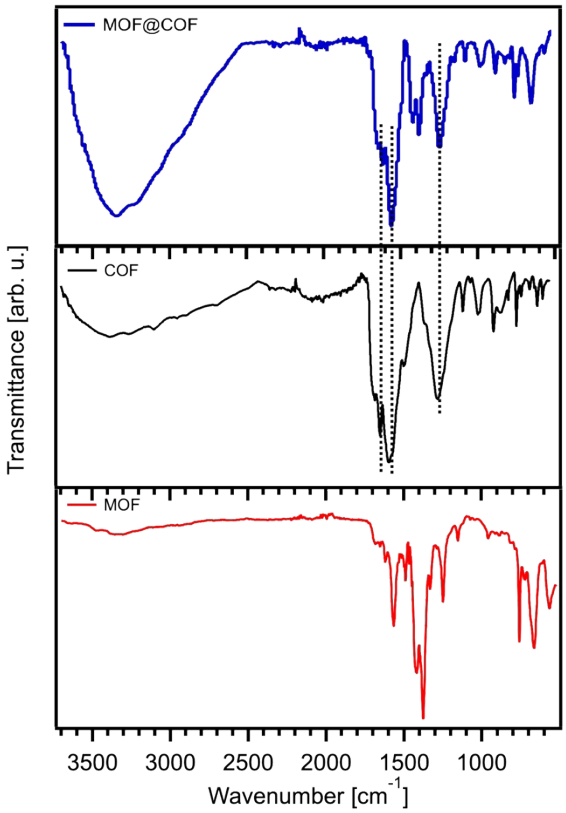

Fig. S3. FT-IR spectra of MOF (UiO-66-NH_2), COF (TFP-TABQ), MOF@COF (UiO-66-NH_2@ TFP-TABQ).

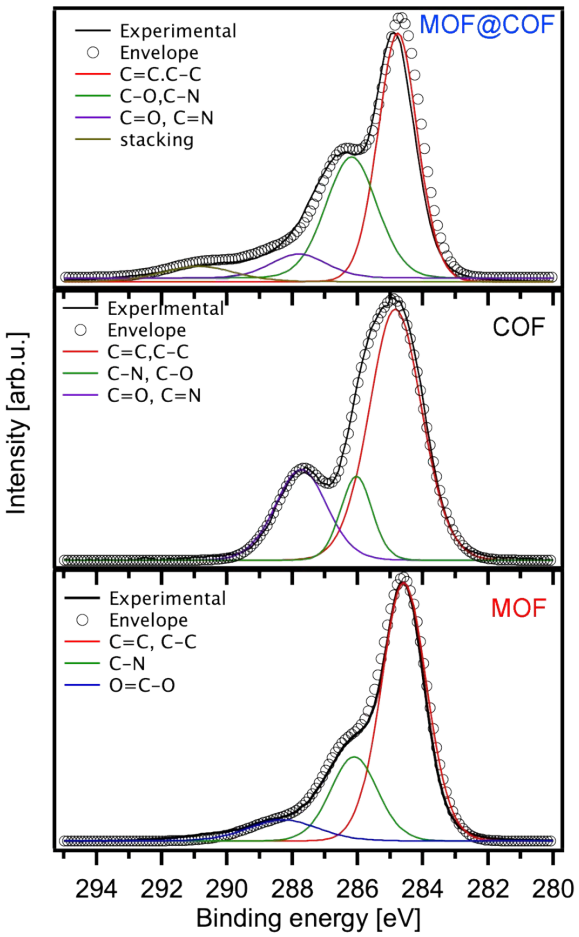

Fig. S4. C1s XPS of MOF, COF and MOF@COF hybrid.

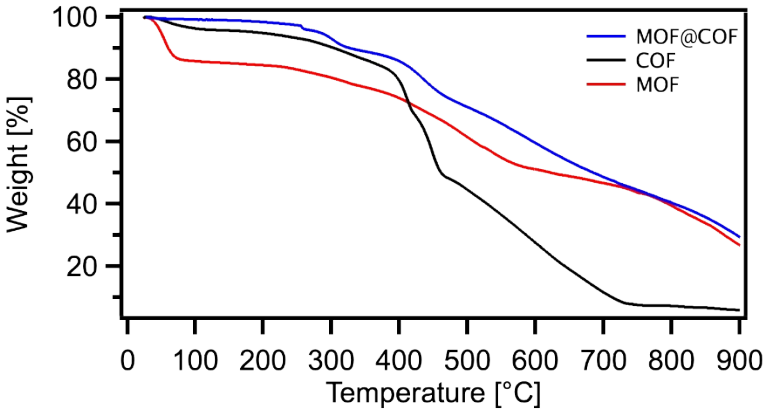

Fig. S5. TGA of MOF, COF and MOF@COF hybrid.

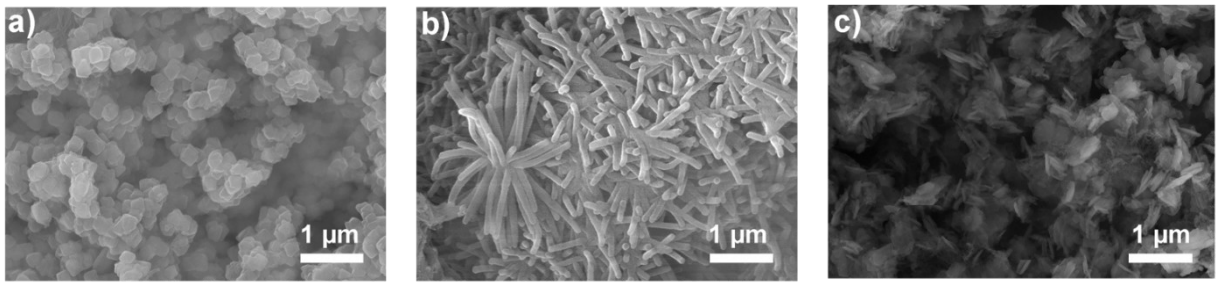

Fig. S6. SEM images of a) MOF, b) COF and c) MOF@COF materials.

Section C. Electrochemical characterization

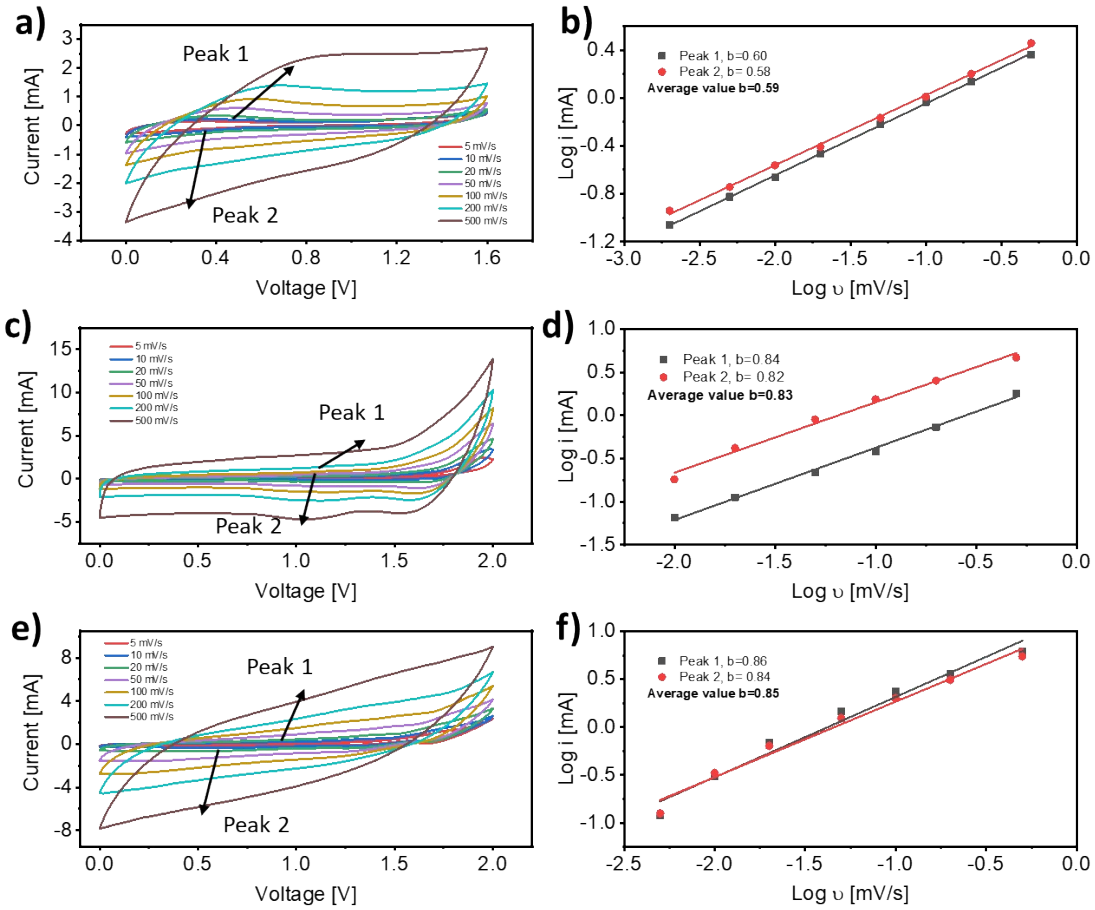

Fig. S7. Electrochemical kinetics study of MOF, COF and MOF@COF. (a, c, e) CV curves at various scan rates for (a) MOF, (c) COF and (e) MOF@COF, (b, d, f) the linear fits of log I vs log v plots to calculate b values according to the equation of $i=av^b$ for (b) MOF, (d) COF and (f) MOF@COF.

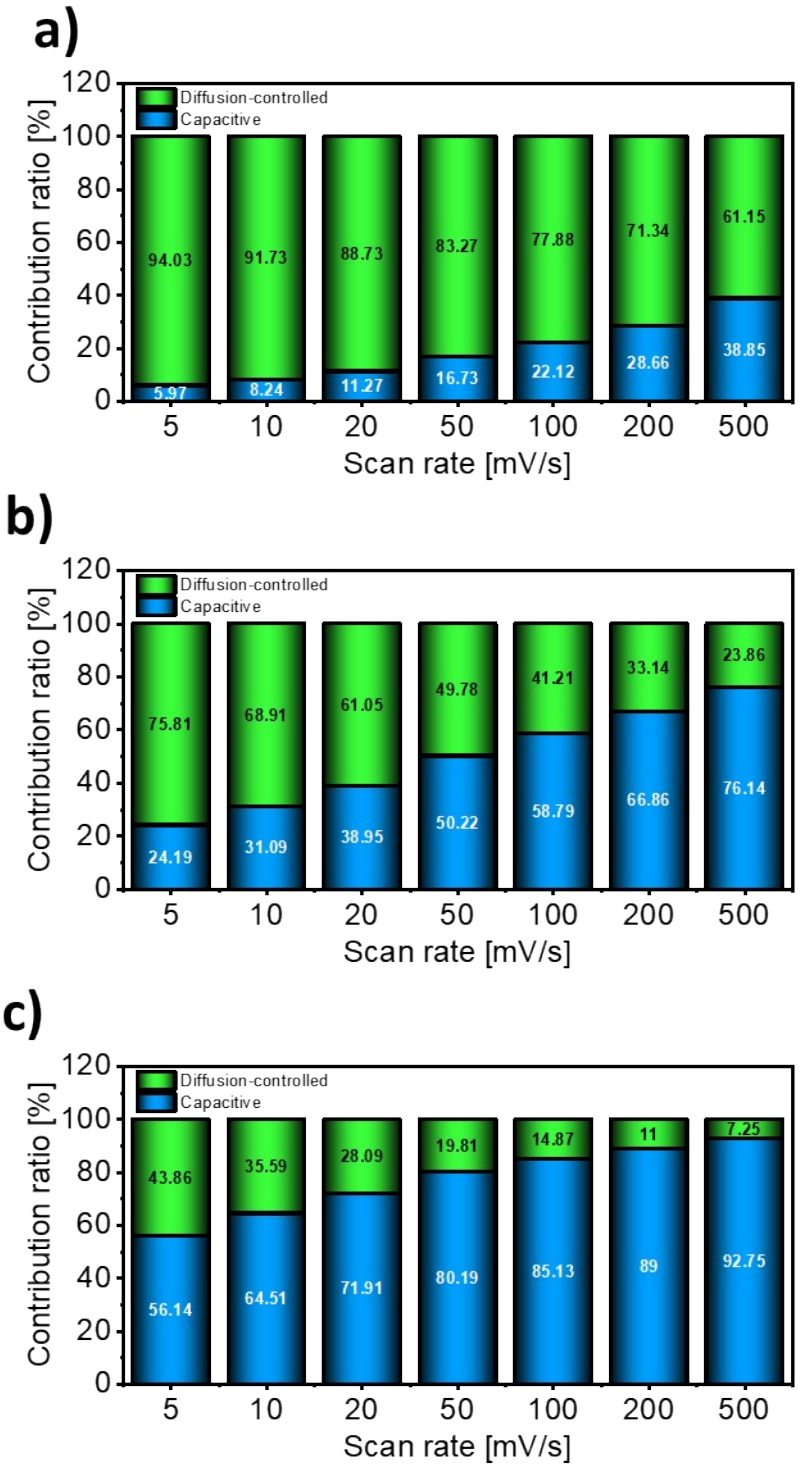

Fig. S8. Capacitive (contribution) and diffusion-controlled contribution of (a) MOF, (b) COF and (c) MOF@COF at various scan rates.

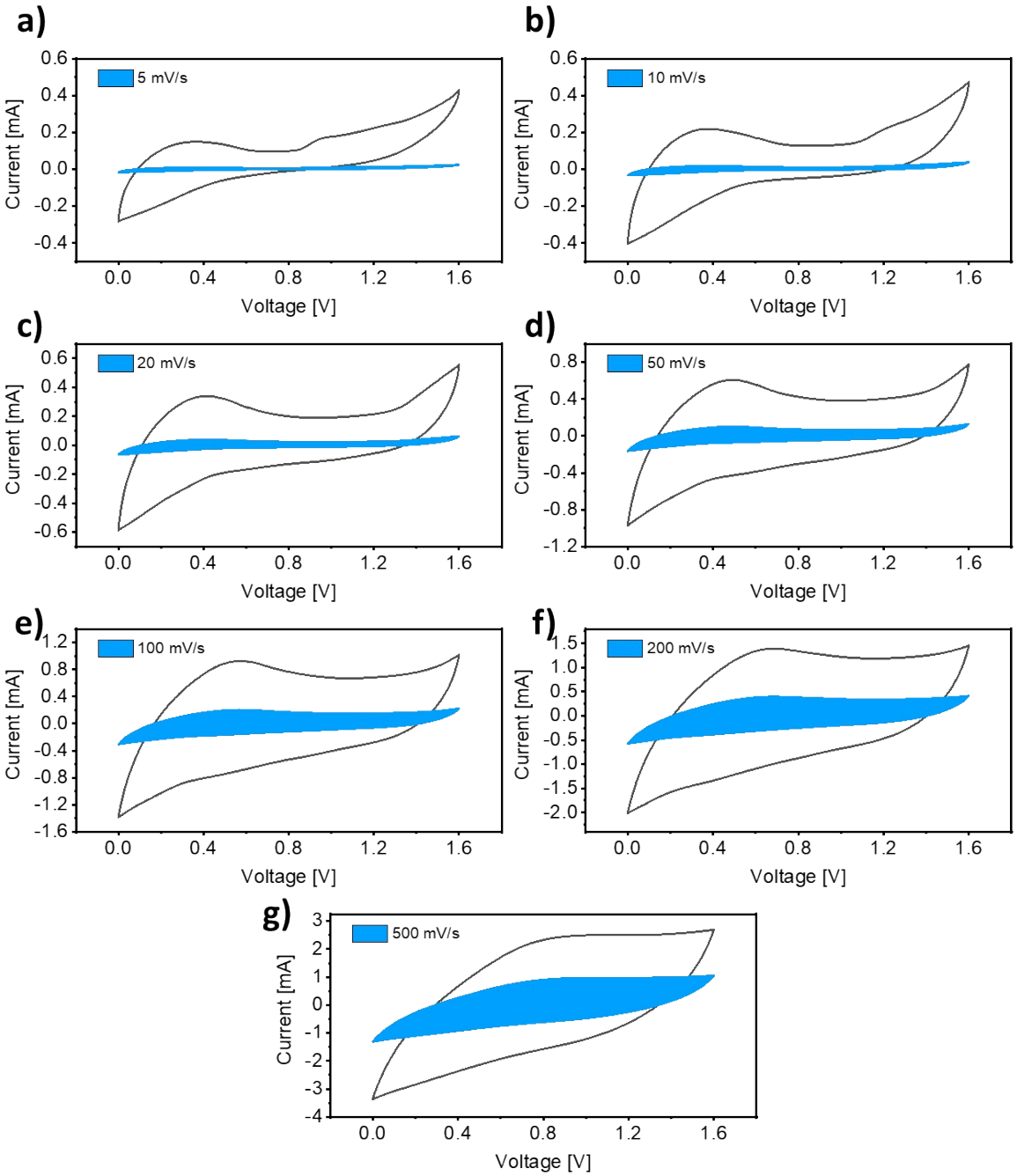

Fig S9. Capacitive (contribution) and diffusion-controlled contribution fraction for the CV curves at various scan rates for MOF.

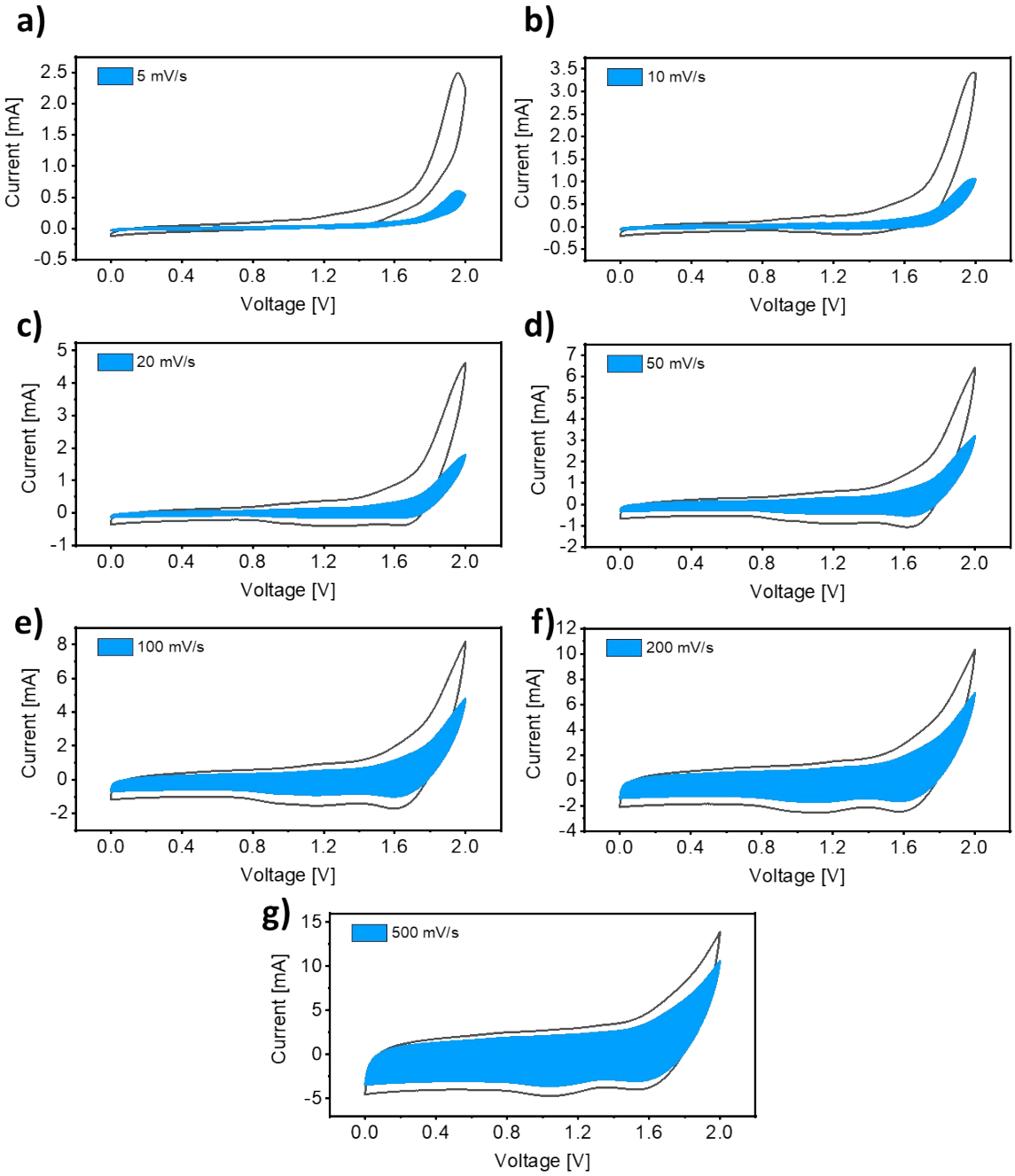

Fig. S10. Capacitive (contribution) and diffusion-controlled contribution fraction for the CV curves at various scan rates for COF.

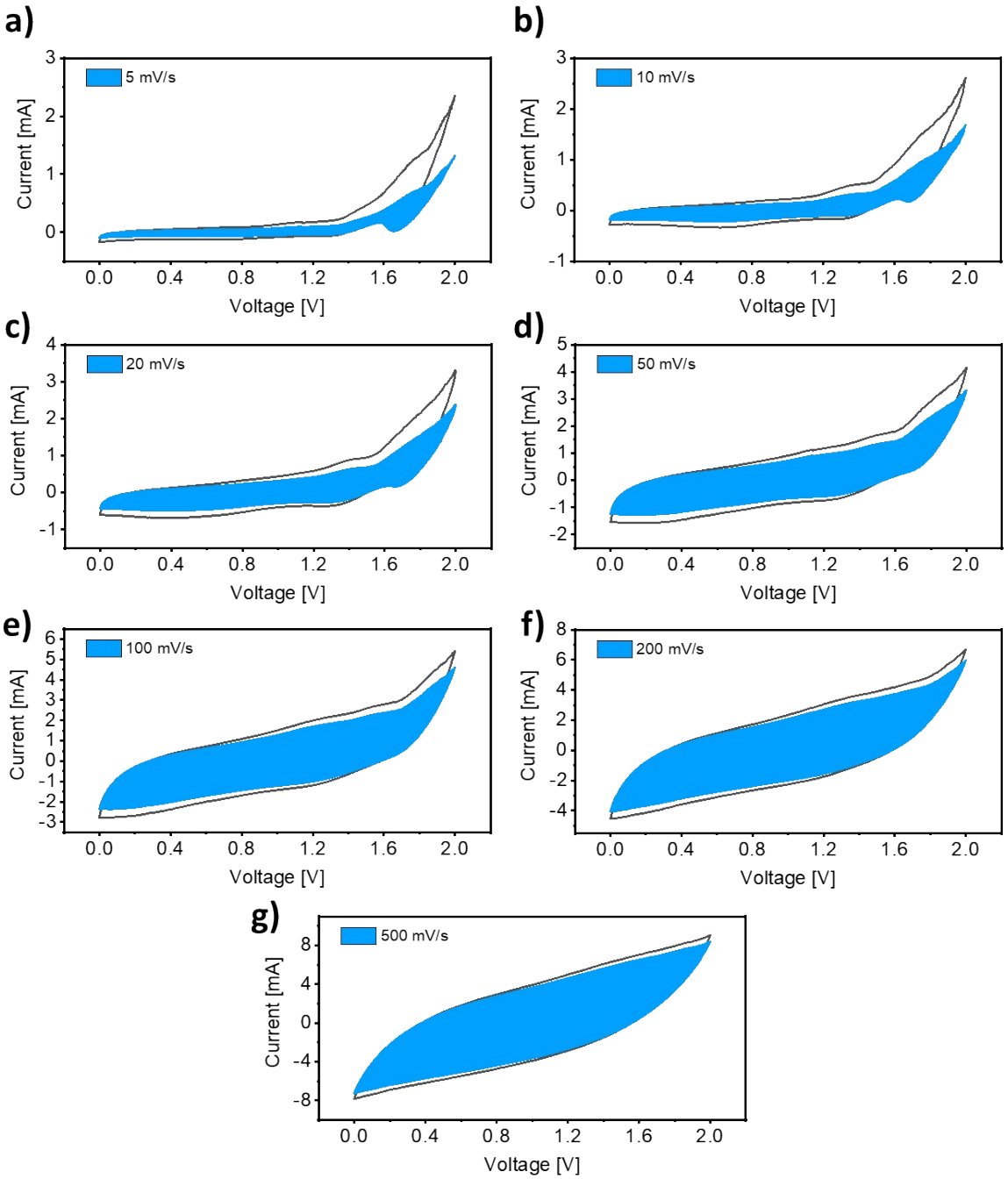

Fig. S11. Capacitive (contribution) and diffusion-controlled contribution fraction for the CV curves at various scan rates for MOF@COF.

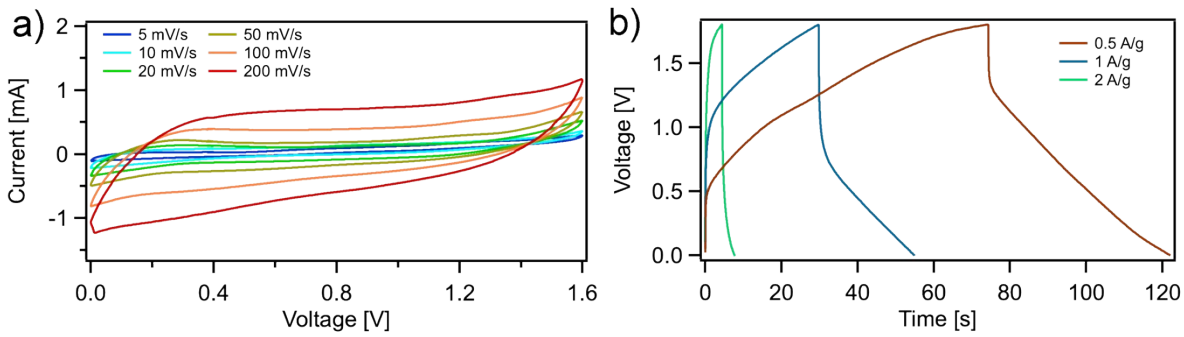

Figure S12 a) CV and b) GCD of UiO-66-NH_2-TFP.

Table S1. Physical parameters and capacitance of MOF, COF and MOF@COF hybrid.

Parameter	MOF	COF	MOF@COF
Surface area (m^2/g)	478	39	236
Average pore size (nm)	0.3	0.9	1.3
Ionic conductivity (S/m)	0.03	0.07	0.15
Crystalline	Yes	Yes	Yes
Redox activity	No	Yes	Yes
Chemical stability	Low	High	High
Capacitance (F/g)	19	58	103

As indicated in Table S1, the electrochemical performance aligns with the trend: MOF < COF < MOF@COF, consistent with most physical parameters, except for surface area. Despite the MOF exhibiting the highest surface area, its subpar porosity, limited ionic conductivity, and absence of redox activity contribute to its inferior electrochemical performance. This underscores a conclusive demonstration that fully harnessing the potential of MOF requires its hybridization with COF.

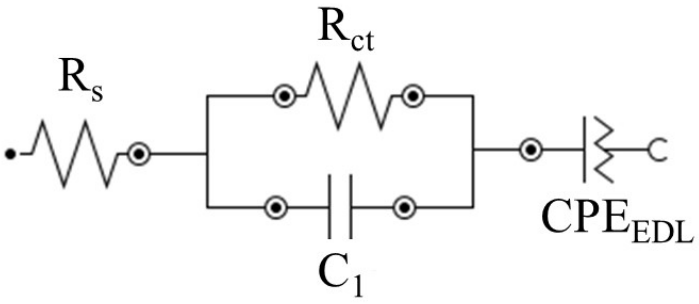

Fig. S13. The equivalent electric circuit models used for fitting the Nyquist plots. R_s: the intrinsic ohmic resistance; R_{ct}: charge transfer resistance; C_1: capacitance element; CPE_{EDL}: constant phase element representing the electrical double layer capacitance (EDLC).

Table S2. Fitting parameters obtained from the Nyquist plots.

Sample	Ri (Ω)	Rct (Ω)	σ (S/m)
MOF	30.98	57.86	0.03
COF	11.11	113.57	0.07
MOF@COF	5.30	2.63	0.15

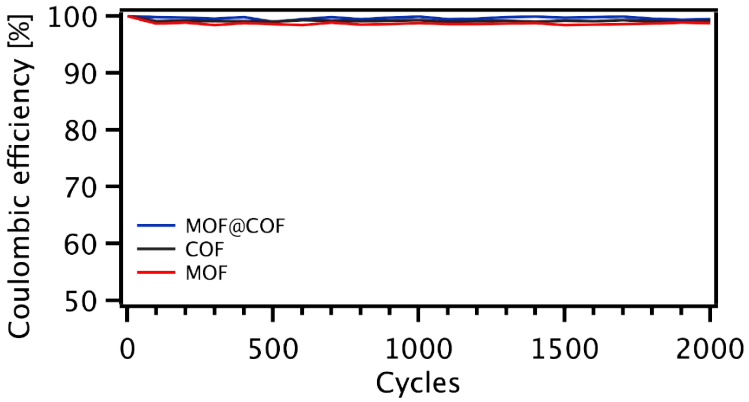

Fig. S14. Coulombic efficiency under 2000 charge/discharge cycles.

Table S3 State of the art of the electrochemical performance of different COFs and MOFs, electrodes as energy storage systems.

Electrode		Surfaces area (m^2/g)	Av. pore size (nm)	Electrolyte	Current density A g^{-1}	Specific capacitance F g^{-1}	Cycle no.	Energy density Wh/kg	Power density kW/kg	Ref.
COF	PDT-COF	312.6	1.8	0.5 M H_2SO_4	1	104	5000 (90%)	32.55	1.88	[1]
	PI-COF	375	1.8	1 M LITFSI	0.5	163	-	35.7	0.25	[2]
	TpPa-COF@PANI	574.4	1.3	1 M H_2SO_4	0.2	95	30 000 (~83%)	-	-	[3]
	BIBDZ-imide COF	177.1	3.1	1M H_3PO_4	0.5	88.4	5000 (93.61%)	12.3	0.25	[4]
	TaPa-Py COF/rGO-30	203	1.5	1 M H_2SO_4	0,5	138	10000 (96%)	20.1	0.25	[5]
	TpOMe-DAQ COF	1735	2.1	H_2SO_4/PVA gel	0.25	84	50000 (65%)	2.9	0.06	[6]
	TFP-TABQ	**39**	**0.9**	**1M EMIMCl**	**0.5**	**58**	**2000 (80%)**	**32.2**	**1.28**	**This work**
MOF	NiCo-$(PTA)_{0.8}(BTC)_{0.2}$ nanosheets	-	-	1 M KOH	1	113	10 000 (97.7%)	40	0.85	[7]
	Co-MOF	489	0.8	1M LiOH	0.6	206	1000 (98.5 %)	7.2	0.16	[8]
	HKUST–1 derived HPCF	620	3.2	6M KOH	2	194.8	10000 (95%)	9.1	3.5	[9]
	Mesoporous $NiCo_2O_4$@MnO_2	501	3-5	1M NaOH	1	112	1000 (98.8%)	35.5	-	[10]

	Cu-MOF	1321	1.3	1M H2SO4	0.5	104.8	10000 (87 %)	18.2	0.81	[11]
	Zr-MOF	720	1.3	1M H2SO4	0.5	70.5	5000 (81%)	14.4	0.84	
	UiO-66	490	1	6M KOH	0.2	101.5	-	32	0.24	[12]
	MOF-UiO-66-NH_2	**478**	**0.3**	**1M EMIMCl**	**0.5**	**19**	**2000 (66%)**	**6.75**	**0.87**	**This work**
MOF@ COF	**UiO-66-NH_2@TFP-TABQ**	**236**	**1.3**	**1M EMIMCl**	**0.5**	**103**	**2000 (95%)**	**57.2**	**1.02**	**This work**

References

1. S. Halder and C. Chakraborty, *ACS Applied Engineering Materials*, 2023, **1**, 1799-1808.
2. R. Iqbal, A. Badshah, Y.-J. Ma and L.-J. Zhi, *Chinese Journal of Polymer Science*, 2020, **38**, 558-564.
3. S. Liu, L. Yao, Y. Lu, X. Hua, J. Liu, Z. Yang, H. Wei and Y. Mai, *Materials Letters*, 2019, **236**, 354-357.
4. A. Roy, S. Mondal, A. Halder, A. Banerjee, D. Ghoshal, A. Paul and S. Malik, *European Polymer Journal*, 2017, **93**, 448-457.
5. C. Wang, F. Liu, S. Yan, C. Liu, Z. Yu, J. Chen, R. Lyu, Z. Wang, M. Xu, S. Dai, Y. Chen and L. Wei, *Carbon*, 2022, **190**, 412-421.
6. A. Halder, M. Ghosh, A. Khayum M, S. Bera, M. Addicoat, H. S. Sasmal, S. Karak, S. Kurungot and R. Banerjee, *J. Am. Chem. Soc.*, 2018, **140**, 10941-10945.
7. S. Huang, X.-R. Shi, C. Sun, X. Zhang, M. Huang, R. Liu, H. Wang and S. Xu, *Applied Surface Science*, 2022, **572**, 151344.
8. D. Y. Lee, S. J. Yoon, N. K. Shrestha, S.-H. Lee, H. Ahn and S.-H. Han, *Microporous and Mesoporous Materials*, 2012, **153**, 163-165.
9. Y. Liu, G. Li, Y. Guo, Y. Ying and X. Peng, *ACS Applied Materials & Interfaces*, 2017, **9**, 14043-14050.
10. L. Yu, G. Zhang, C. Yuan and X. W. Lou, *Chemical Communications*, 2013, **49**, 137-139.
11. P. Dubey, V. Shrivastav, P. H. Maheshwari, M. Hołdyński, A. Krawczyńska and S. Sundriyal, *Journal of Energy Storage*, 2023, **68**, 107828.
12. W. Gao, D. Chen, H. Quan, R. Zou, W. Wang, X. Luo and L. Guo, *ACS Sustainable Chemistry & Engineering*, 2017, **5**, 4144-4153.